

# An Investigation on Rotating Stall in an Aeroengine Transonic Compressor with Inlet Distortion



Zhongyu Zhu and Xiaohua Liu

**Abstract** The internal flow stability of the compressor in the aeroengine has always been the top priority for the development of the aviation industry. Rotating stall is one of the most common instability problems in compressors, and stall margin is also an important parameter to measure the aerodynamic performance of compressors. In an actual compressor, it is difficult to achieve an ideal uniform inlet air condition, and inlet distortion will affect the operating conditions of the compressor. In this paper, a three-dimensional simulation of rotor 37 is conducted to study the development process of circumferential distortion and the aerodynamic performance of the compressor. The research results show that as the backpressure increases in the channel corresponding to the circumferentially distorted area, the blockage will occur first, and it will develop in the whole channel, leading to a complete stall. From the perspective of aerodynamic performance, circumferential distortion has an impact on stall margin and adiabatic efficiency, and different types of circumferential distortion have different effects on aerodynamic performance.

**Keywords** Rotating stall · Circumferential distortion · Numerical simulation

## 1 Introduction

As one of the core components of aeroengine, compressor is the main component that provides thrust. The problems of flow stability inside compressor seriously limit the development of aeroengine. In fact, every major breakthrough in aeroengine technology is closely related to the breakthrough in compression technology. Therefore,

---

Z. Zhu · X. Liu (✉)  
Shanghai Jiao Tong University, Shanghai, China  
e-mail: [Xiaohua-Liu@sjtu.edu.cn](mailto:Xiaohua-Liu@sjtu.edu.cn)

Z. Zhu  
e-mail: [zzy123@sjtu.edu.cn](mailto:zzy123@sjtu.edu.cn)

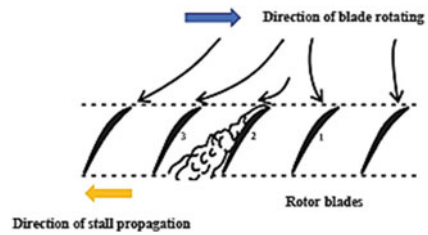
Key Laboratory (Fluid Machinery and Engineering Research Base) of Sichuan Province, Chengdu, China

in the pursuit of high-pressure ratio and high efficiency, it is very necessary to ensure the stable operation of the compressor under various conditions. The corresponding quantity reflecting the stable working range of the compressor is the stall margin. Stall margin is one of the important indicators to measure the design of a compressor. It not only reflects the performance of the compressor, but also determines whether it can be actually used.

The unsteady flow stability problem in compressor mainly includes surge and rotating stall. These unstable conditions will cause the rotor to break away from the original speed, reduce the pressure ratio and efficiency, and even cause the damage of the blade and compressor. In terms of rotating stall, researchers mainly focused on theoretical research and engineering applications. On the one hand, from the perspective of theoretical research, since the 1950s, a large number of scholars at home and abroad began to study this problem [1]. They mainly focused on the development process of stall mass, trying to explain the stall phenomenon from a theoretical point of view. The size of the stall group, the propagation speed, and the hysteresis of exiting the stall after the stall are the hotspots of research. On the other hand, in the actual process, people are more concerned about how to determine the stable working range of a compressor, that is, accurately predict the starting position of the stall. CFD steady calculations converge to obtain a specific flow pattern, and it is stable only under certain small disturbances. In order to be able to adapt to various disturbances, researchers began to seek new stability models [2]. The new stall stability model is based on the theory of small disturbances. It is believed that the compressor's response to small disturbances in the flow field develops linearly before stalling. On this basis, two-dimensional and three-dimensional models for different environments are developed [3]. In the numerical simulation of inlet distortion, considering the complexity of the flow field in the actual compressor, the numerical simulation of inlet distortion is actually difficult to completely restore. Therefore, people often only choose total pressure, total temperature, or swirl flow as a specific type of distortion, and then set the distortion area and distortion intensity, and then study the aerodynamic performance of the compressor under the distortion.

Till now, with the advancement of science and technology, people's research on rotating stalls and the observation of phenomena have deepened the discussion of its internal mechanism and prediction methods. The capture of spike-type stalls has become more and more along with the development of sampling technology. In terms of numerical simulation, with the development of CFD software and computer performance, researchers have become more and more reducible to the real working conditions of the compressor, and the calculation speed and accuracy have been significantly improved. This article aims to explain the phenomenon and principle of rotating stall and inlet distortion. Based on ANSYS-CFX, the ROTOR37 is numerically simulated. We observed the development process of stall under the condition of circumferential distortion, and the aerodynamic performance of the compressor half-stage is also studied.

**Fig. 1** Schematic diagram of rotating stall principle



## 2 The Phenomenon of Rotating Stall and Inlet Distortion

### 2.1 Rotating Stall

When the speed is constant and the airflow is reduced, the angle of attack of the rotor blades will increase. When the airflow is reduced to a certain level, an unstable flow will be observed, and the compressor will make a special cry and the vibration will increase [4]. The flow field measured behind the moving blade shows that there are one or more low-speed airflow zones rotating along the rotating direction of the moving blade at a certain speed. This unstable condition is called a rotating stall. In other words, Rotational stall is a localized disruption of airflow within the compressor, which continues to deliver compressed air, but at a lower efficiency. Rotational stall is an example of compressor instability that can have catastrophic consequences for an aircraft engine. Jammed airfoils create pockets of relatively stagnant air (called stall cells) that rotate around the circumference of the compressor instead of moving in the direction of flow. The stall cells rotate with the rotor blades, but at a speed of 50–70% of their speed, acting on subsequent aerodynamic surfaces around the rotor when each of them collides with the stall cell. The propagation of instability around the annular space of the flow path is caused by blockage of the stall cell, causing a blowout to an adjacent blade. The adjacent vane is stopped by the shock of the fall, causing the stall cell to “spin” around the rotor [5], as is shown in Fig. 1.

### 2.2 Inlet Distortion

In a broad sense, for a single component or engine, all inlet conditions that deviate from the uniform and steady state can be regarded as inlet distortion [6]. Inlet distortion will cause the relevant components and the engine to deviate from the expected operating point.

From the perspective of the non-uniform distribution of aerodynamic parameters, the inlet distortion can be roughly divided into four types: total pressure distortion, total temperature distortion, swirl distortion, and rotation distortion. In the actual process, the measurement of the aerodynamic non-uniformity at the inlet section is much more convenient than the measurement of the aerodynamic parameters at the

inlet of the blade row or between the stages. The total temperature and total pressure usually do not change much during the airflow transmission along the inlet, so in engineering, total temperature and total pressure are usually selected as the basis for judging distortion.

Total pressure distortion is the most common and most studied distortion method. Total temperature distortion generally occurs in military aircraft and is usually caused by the inhalation of high-temperature exhaust gas. Swirl distortion is usually caused by the secondary flow caused by the turning of the inlet [7]. When flowing in a curved pipe, it is subject to centrifugal force. The centrifugal force points to the outside of the curved pipe. Therefore, when the fluid flows along the axis of the pipe, it will also flow to the outside of the curved pipe under the action of centrifugal force. The centrifugal force is also large, so it flows outward at a higher secondary flow velocity; rotation distortion usually occurs in multi-stage or multi-axis compressors. When the upstream blade row stalls, the stall group spreads circumferentially. The blade row is a kind of circumferential total pressure distortion. For the convenience of research, the distortion is usually artificially divided into radial distortion and circumferential distortion. Radial distortion means that the aerodynamic parameters only change in the radial direction and are uniform in the circumferential direction. The circumferential distortion is just the opposite, as shown in Fig. 2. Strictly speaking, the actual situation is usually a compound distortion of these two kinds [8].

For different types of inlet distortion, researchers have invested a lot of energy in experimental exploration. In the actual experimental operation, the researchers designed various forms of distortion generators, as shown in the following Fig. 3

**Fig. 2** Schematic diagram of F radial distortion and circumferential distortion **a** Radial distortion, **b** Circumferential distortion

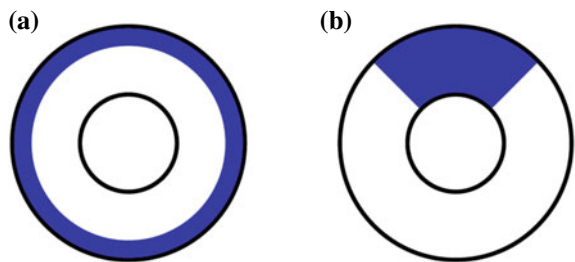
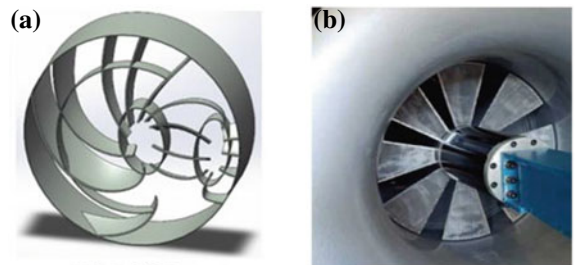


**Fig. 3** Common distortion generator [9] **a** swirl distortion generator, **b** rotating distortion generator



[9], and installed them in different positions of the engine to simulate the different distortion conditions encountered during the operation of the compressor.

### 3 Governing Equations and Turbulence Models

#### 3.1 Governing Equations

This paper adopts the Navier–Stokes equation of Reynolds average, which can be expressed as

$$\frac{\partial}{\partial t} \int_{\Omega} U d\Omega + \int_S \vec{F}_I \cdot d\vec{S} + \int_S \vec{F}_V \cdot d\vec{S} = \int_{\Omega} S_T d\Omega, \quad (1)$$

where  $\Omega$  represent volume,  $S$  represent square,  $U$  represent the conserved parameter,  $\vec{F}_I$  and  $\vec{F}_V$ , respectively, represent inviscid vector flux and viscous vector flux.  $S_T$  is the source term, and its expression is

$$U = \begin{bmatrix} \rho \\ \rho v_1 \\ \rho v_2 \\ \rho v_3 \\ \rho E \end{bmatrix}, \quad F_{li} = \begin{bmatrix} \rho v_i \\ \rho v_1 v_i + p \delta_{1i} \\ \rho v_2 v_i + p \delta_{2i} \\ \rho v_3 v_i + p \delta_{3i} \\ (\rho E + p) v_i \end{bmatrix}, \quad F_{vi} = - \begin{bmatrix} 0 \\ \tau_{i1} \\ \tau_{i2} \\ \tau_{i3} \\ q_i + v_j \tau_{ij} \end{bmatrix}, \quad S_T = \begin{bmatrix} 0 \\ \rho f_{e1} \\ \rho f_{e2} \\ \rho f_{e3} \\ W_f \end{bmatrix}, \quad (2)$$

where the total energy and heat flux can, respectively, be expressed as

$$E = e + \frac{1}{2} v_i v_i \quad (3)$$

$$q_i = \kappa \frac{\partial}{\partial x_i} T. \quad (4)$$

In the above formula,  $\kappa$  is the laminar heat transfer coefficient,  $\rho f_{e1}$ ,  $\rho f_{e2}$ ,  $\rho f_{e3}$  are the components of the external force  $\vec{f}_e$ , and  $W_f$  is the work done by the external force.

$$W_f = \rho \vec{f}_e \cdot \vec{v}. \quad (5)$$

In order to close the Navier–Stokes equation, the definition of the shear stress tensor must be given according to other flow variables. Only Newtonian fluid is

considered here, and its shear stress tensor is given by

$$\tau_{ij} = \mu \left[ \left( \frac{\partial v_j}{\partial x_i} + \frac{\partial v_i}{\partial x_j} \right) - \frac{2}{3} (\nabla \cdot \vec{v}) \delta_{ij} \right]. \quad (6)$$

Among them,  $\mu$  is the viscosity coefficient, and  $\delta_{ij}$  is the Kronecker symbol.

$$\delta_{ij} = \begin{cases} 0, & \text{if } i \neq j \\ 1, & \text{if } i = j \end{cases}. \quad (7)$$

### 3.2 Turbulence Models

The turbulence model is based on the time-averaged Navier–Stokes equation. In the numerical calculation process, different turbulence models will get different results. Therefore, it is necessary to select a suitable turbulence model according to actual needs. Commonly used turbulence models include Baldwin–Lomax zero equation model, Spalart–Allmaras one equation model, SARC one equation model, k-epsilon two-equation model, SST two-equation model, k-omega two-equation model, v2-f four equation model, and EARSM algebraic Reynolds stress model. In this paper, the Spalart–Allmaras (S-A) one equation model is selected for numerical calculation.

The S-A turbulence model is based on the solution of the vortex viscous migration equation, can handle more complex flows, has good robustness, and has low CPU and memory requirements. In 1992, Spalart and Allmaras [10] proposed the solution process of the S-A turbulence model. In 1996, Ashford and Powell [11] supplemented the theory.

The turbulent viscosity coefficient of the S-A model is

$$\nu_t = \tilde{\nu} f_{v1} \quad (8)$$

Among them,  $\tilde{\nu}$  is the turbulence working variable,  $f_{v1}$  is defined as follows:

$$f_{v1} = \frac{\chi^3}{\chi^3 + c_{v1}}. \quad (9)$$

Among them,  $\chi$  is the ratio of the turbulent working variable  $\tilde{\nu}$  to the molecular viscosity  $\nu$

$$\chi = \frac{\tilde{\nu}}{\nu}. \quad (10)$$

The turbulent working variable  $\tilde{\nu}$  obeys the migration equation shown below.

$$\frac{\partial \mathbf{v}}{\partial t} + \tilde{\mathbf{V}} \cdot \nabla \tilde{\mathbf{v}} = \frac{1}{\sigma} \left\{ \nabla \cdot \left[ (\mathbf{v} + (1 + c_{b2})\tilde{\mathbf{v}})\nabla \tilde{\mathbf{v}} \right] - c_{b2}\tilde{\mathbf{v}}\Delta \tilde{\mathbf{v}} \right\} + S_T. \quad (11)$$

Among them,  $\sigma$ ,  $c_{b2}$  are constants,  $\mathbf{V}$  is the velocity vector,  $S_T$  is the source term, and the source term includes the generation term  $S_T$  and the dissipation term  $f_w$ .

$$S_T = \tilde{\mathbf{V}}P(\tilde{\mathbf{v}}) - \tilde{\mathbf{V}}D(\tilde{\mathbf{v}}). \quad (12)$$

Inside the equation:

$$\tilde{\mathbf{v}}P(\tilde{\mathbf{v}}) = c_{b1}S\tilde{\mathbf{v}} \quad (13)$$

$$\tilde{\mathbf{v}}D(\tilde{\mathbf{v}}) = c_{w1}f_w \left( \frac{\tilde{\mathbf{v}}}{d} \right)^2. \quad (14)$$

The generating term  $P$  is related to the following formula.

$$\tilde{S} = Sf_{v3} + \frac{\tilde{\mathbf{V}}}{k^2d^2}f_{v2} \quad (15)$$

$$f_{v2} = \frac{1}{(1 + \chi/c_{v2})^3} \quad (16)$$

$$f_{v3} = \frac{(1 + \chi f_{v1})(1 - f_{v2})}{\chi}. \quad (17)$$

Among them,  $d$  is the minimum distance from the wall, and  $S$  is the vortex intensity. The dissipation term  $f_w$  is

$$f_w = g((1 + c_w3^6)/(g^6 + c_w3^6))^{(1/6)}. \quad (18)$$

Inside the equation:

$$g = r + c_{w2}(r^6 - r) \quad (19)$$

$$r = \frac{\tilde{\mathbf{v}}}{\tilde{S}k^2d^2}. \quad (20)$$

The constant term in the model is

$$c_{w1} = \frac{c_{b1}}{k^2} + \frac{(1 + c_{b2})}{\sigma}, c_{w2} = 0.3, c_{w3} = 2, c_{v1} = 7.1, c_{v2} = 5, \\ c_{b1} = 0.1355, c_{b2} = 0.622, k = 0.41, \sigma = 2/3. \quad (21)$$

## 4 Numerical Simulation of Circumferential Distortion

### 4.1 Compressor Description

Rotor37 is a transonic compressor rotor designed by NASA-Lewis Research and Design Center. Uder et al. [12] conducted a detailed experimental test on this rotor. The test measurement position is shown in Fig. 4. The flow results (Table 1) used in this paper are taken from the position 1 and 4.

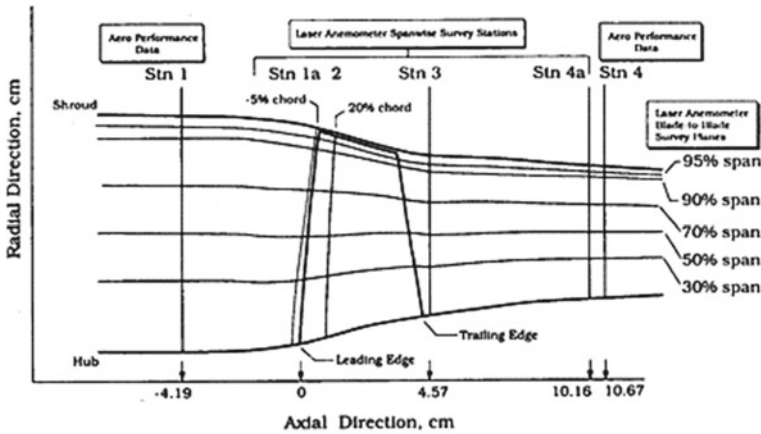


Fig. 4 Positions of measurement station of Rotor37 [14]

Table 1 Main design parameters of Rotor37 [13]

Parameter	Value
Blade number	36
Hub-tip ratio	0.7
Aspect ratio	1.19
Tip consistency	1.29
Rotor tip clearance (mm)	0.356
Rotational speed (r/min)	17,188
Tip tangential velocity (m/s)	454.14
Total pressure ratio	2.106
Total temperature ratio	0.877
Design point mass flow (kg/s)	20.19
Choking point mass flow (kg/s)	20.93



## 4.2 Computational Mesh and Boundary Conditions

The simulation of this paper was conducted by the commercial computational fluid dynamics software ANSYS-CFX. In order to meet the characteristics of uneven circumferential distortion in the circumferential direction, we have selected the full passage as the calculation domain for numerical calculation, as is shown in Fig. 5. The applied grid consists of 14,400,000 nodes. There are 44 nodes in blade spanwise direction including 7 nodes in blade tip clearance. The grid topology is of HOH-type, with the O-type mesh generated around the rotor and the H-type mesh in inlet and outlet. In order to meet the requirement of S-A turbulence model, the  $y^+$  adjacent to the solid wall was set as 5. To verify the feasibility of the calculation grid, we compared the steady flow calculation results under this grid setting method with the experimental data. It can be found that the calculated results under this grid condition are very close to the actual experimental results, as is shown in Fig. 6. Due to the limitation of calculation conditions, we can think that this kind of 14,400,000-node grid can more accurately reflect the situation of the flow field.

As for the design of circumferential distortion, two different circumferential distortions are designed for comparison. The first case is to simulate the situation

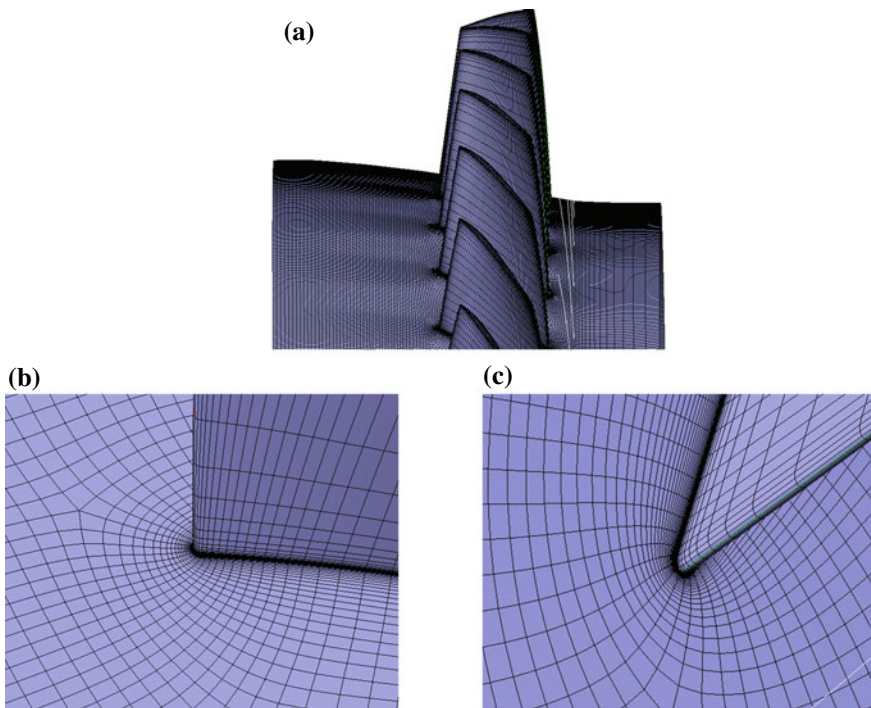


**Fig. 5** Different perspectives of the computing grid

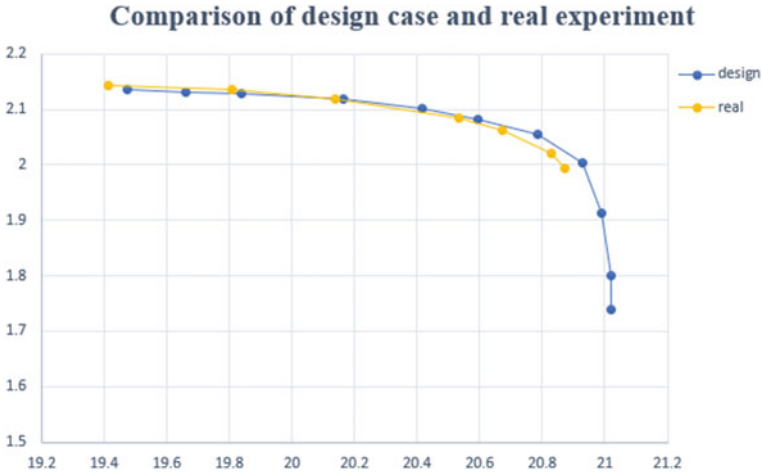


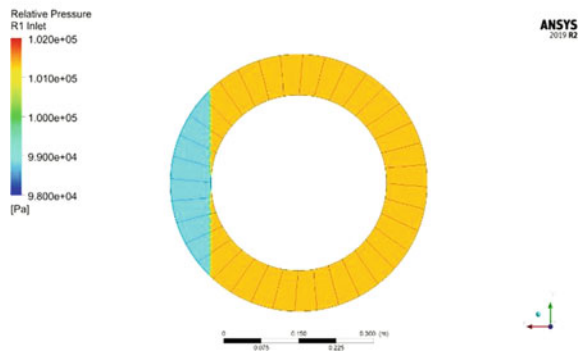
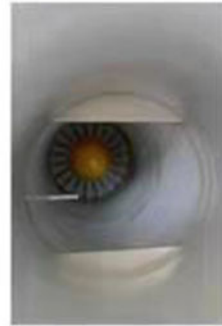
**Fig. 6** Comparison of design case and real experiment

of inserting the baffle in the actual experiment. The comparison between the experimental equipment and the numerical simulation effect is shown in Fig. 7. The other case is related to distortion angle. In order to control the area of the two cases to be equal, through calculation, we set the distortion angle as  $67.7^\circ$ , as is shown in Fig. 8. In both cases, the distortion intensity of the distortion area is 2500 Pa. Moreover, we will call these two cases flashboard distortion and angle distortion in the rest part of this paper.

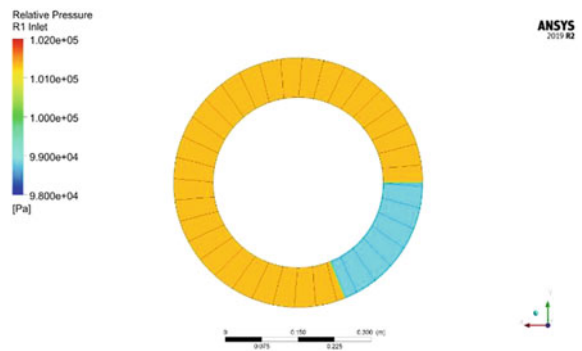
### 4.3 Influence on Compressor Performance

Figure 9 shows the characteristic line and isentropic efficiency of ROTOR37 with a distorted inlet. From the comparison chart, we can clearly find that the influence of the circumferential distortion on the aerodynamic performance of the two cases is similar. Circumferential distortion has attenuated the flow rate and total pressure ratio of the blocking point, and the flow position of the peak efficiency point of the adiabatic efficiency has also moved downward. It can be found that the adiabatic efficiency also has a small drop, but it may not be very obvious due to the distortion area and even if the length is not large enough. At the same time, comparing the circumferential distortion data in the two cases, it can be found that the plug-in circumferential distortion has a greater impact on the efficiency, and the efficiency at the peak is about 0.03% less than the angle distortion. The stall margin of angle circumferential distortion is 10.686%, and the stall margin of insert plate distortion is 11.144%, which is about 0.5% higher than the former. Therefore, it can be inferred

**Fig. 7** Comparison of the experiment and the numerical simulation

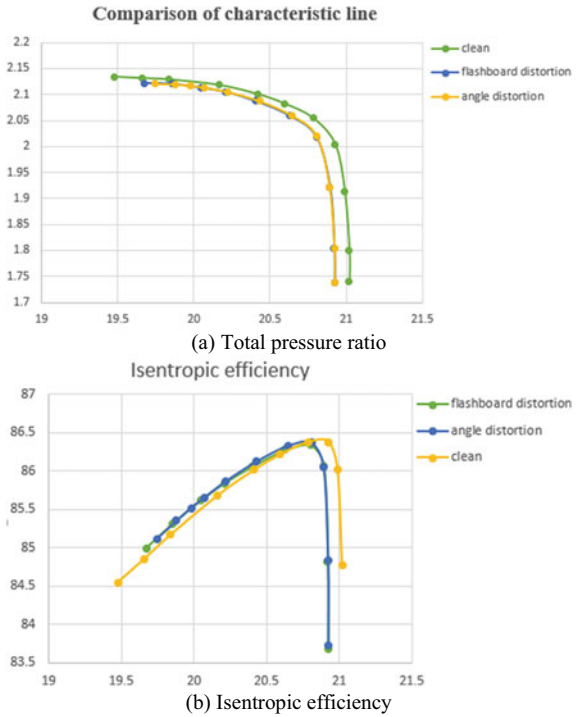


**Fig. 8** Numerical simulation of angle distortion



that the circumferential distortion of the insert plate is closer to the rim distortion zone, which has a greater impact on the thermal insulation efficiency, while the angle distortion is closer to the hub and has a greater degree of distortion, which has a greater impact on the flow capacity.

**Fig. 9** The characteristic curves of compressors



### 4.4 Development of Rotating Stall

We can see from the last section that under the influence of circumferential distortion, the characteristic line of ROTOR37 has moved downward overall, and the flow rate of the blocking point, stall margin, and adiabatic efficiency have all been attenuated to a certain extent. In order to explore the mechanism of the impact of circumferential distortion on aerodynamic performance, we tried to restore the flow in the channel from the blocking point to the near-stall point. We derive and integrate the blade-to-blade static entropy distribution map at 90% leaf height corresponding to each backpressure situation. As is shown in Figs. 10 and 11, we, respectively, show the development process of the rotation stall in the full channel under the conditions of the flashboard distortion and the angle distortion. The positive direction along the x-axis in the figure is the process from the blocking point to the near-stall point. In each case, the 36 channels are shown as a plan view cut from the middle at 90% span.

We can clearly find that the static entropy of the gas in the channel corresponding to the circumferential distortion zone is significantly higher than that of the channel corresponding to the normal region. With the attenuation of the mass flow in the

**Fig. 10** The development of stall in flashboard distortion

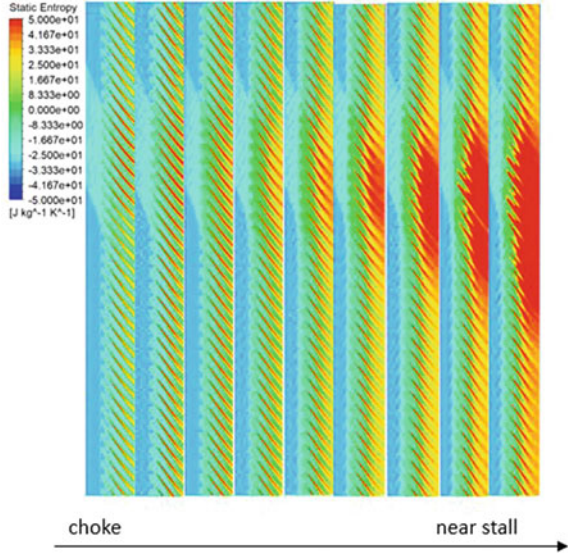
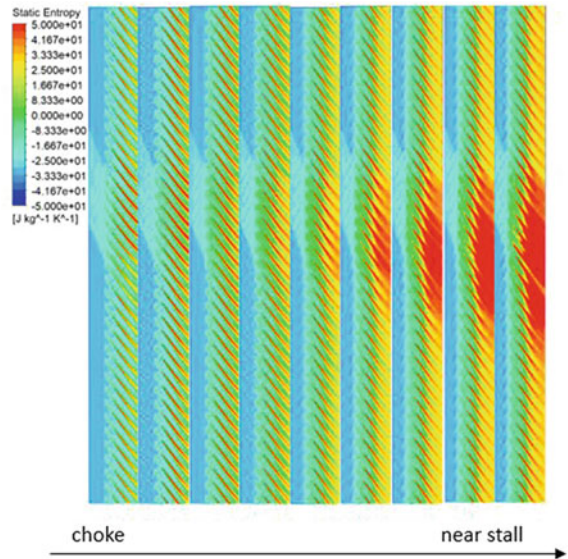


**Fig. 11** The development of stall in angle distortion



passage and the increase of the pressure ratio, the gas disorder in the channel corresponding to the distortion zone increases significantly, and diffuses into the surrounding channels, resulting in a significant increase in the degree of congestion in the blade channel, and finally leading to a complete stall and comparing the two cases, it can be found that although the area of the distortion area is the same, the flashboard distortion depends on the larger area of the receiver, so the number of

channels affected by the distortion is more, and the corresponding area with high entropy in the figure is also larger. However, angle distortion, due to the serious congestion in the channel of the distortion zone, and the larger area of the area close to the hub, has a greater impact on the flow capacity of the compressor.

## 5 Conclusion

As the main complex operating conditions encountered by actual compressors, inlet distortion is of great significance to its research and prevention. With the improvement of calculation conditions, people will pay more attention to the use of simulation methods and conduct research in related fields. In this way, you can use the input conditions to set your own design ideas as you like, and it can also save experimental costs to a large extent.

This paper studies the difference in the impact of the two circumferential distortions on the engine performance and the development process of the rotating stall in the full channel. It can be found that the inlet distortion has a certain negative impact on the overall performance of the compressor. The flow capacity has a greater impact, and more distortion near the rim has a greater impact on efficiency. In addition, observing the rotating stall process under the condition of circumferential distortion, it can be found that the gas in the several channels corresponding to the distortion zone is initially blocked to a certain extent. As the backpressure increases, the degree of blockage in these channels gradually becomes serious and spreads to the surrounding channels, finally leading to the complete development of the stall.

In the future, the study of circumferential distortion will be able to go deep into many aspects, and the significance of its exploration is also significant. On the one hand, there are many forms of circumferential distortion. The total pressure distortion in this article is only a rough restoration of the real situation. The future research on software-recognizable representation methods of complex imported situations will be very valuable. On the other hand, the research on more accurate turbulence models and three-dimensional calculation methods will also be of great significance.

**Acknowledgements** The first author greatly appreciates the support from China Scholarship Council. This work is partially supported by National Natural Science Foundation of China (No.51976116), Natural Science Fund of Shanghai (No.19ZR1425900), and the Open Research Subject of Key Laboratory (Fluid Machinery and Engineering Research Base) of Sichuan Province (No. rszjj2019022).

## References

1. Sears WR (1955) Rotating stall in axial compressors. 6(6):429–455
2. Gong Y, Tan CS, Gordon KA et al (1999) A computational model for short-wavelength stall inception and development in multistage compressors. 121(4):726–734

3. He L (2012) Computational study of rotating-stall inception in axial compressors 13(1)
4. Day IJ (1993) Stall Precursors in Axial Flow Compressors. *J Turbomach* 115(1):1–9
5. Emmons HW, Pearson CE, Grant HP (1955) Compressor surge and stall propagation. *Trans ASME* 77(3):455–469
6. Inoue M, Kuroumaru M, Tanino T et al (2000) Propagation of multiple short-length-scale stall cells in an axial compressor rotor. 122(1):45–54
7. Xu D, He C, Sun D et al (2021) Stall inception prediction of axial compressors with radial inlet distortions. *Aerosp Sci Technol* 109
8. Li F, Li J, Dong X, Sun D, Sun X (2017) Influence of SPS casing treatment on axial flow compressor subjected to radial pressure distortion. *Chin J Aeronaut* 30(02):685–697
9. Dong X et al (2018) Stall margin enhancement of a novel casing treatment subjected to circumferential pressure distortion. *Aerosp Sci Technol* 73:239–255
10. Spalart PR, Allmaras SR (1992) A one equation turbulence model for aerodynamic flows. AIAA-92-0439
11. Ashford GA, Powell KG (1996) An unstructured grid generation and adaptive solution technique for high-reynolds number compressible flow. Von Karman Institute Lecture Series. 1996-06.
12. Suder KL, Chima RV, Strazisar AJ, Roberts WB (1995) The effect of adding roughness and thickness to a transonic axial compressor rotor. *J Turbomach* 117(4):491–505
13. Reid L, Moore RD (1978) Design and overall performance of four highly-loaded, high speed inlet stages for an advanced, high pressure ratio core compressor. NASA-TP-1337
14. Benini E, Biollo R (2006) On the aerodynamics of swept and leaned transonic compressor rotors. In: *Turbo expo: power for land, sea, and air*. Barcelona, Spain